




OPEN HOIL-1L deficiency induces cell cycle alteration which causes immaturity of skeletal muscle and cardiomyocytes

Kentaro Akagi¹, Shiro Baba¹, Hiroaki Fujita², Yasuhiro Fuseya², Daisuke Yoshinaga¹, Hirohito Kubota², Eitaro Kume¹, Fumiaki Fukumura¹, Koichi Matsuda¹, Takayuki Tanaka¹, Takuya Hirata¹, Megumu K. Saito³, Kazuhiro Iwai² & Junko Takita¹

HOIL-1L deficiency was recently reported to be one of the causes of myopathy and dilated cardiomyopathy (DCM). However, the mechanisms by which myopathy and DCM develop have not been clearly elucidated. Here, we sought to elucidate these mechanisms using the murine myoblast cell line C2C12 and disease-specific human induced pluripotent stem cells (hiPSCs). Myotubes differentiated from HOIL-1L-KO C2C12 cells exhibited deteriorated differentiation and mitotic cell accumulation. CMs differentiated from patient-derived hiPSCs had an abnormal morphology with a larger size and were excessively multinucleated compared with CMs differentiated from control hiPSCs. Further analysis of hiPSC-derived CMs showed that HOIL-1L deficiency caused cell cycle alteration and mitotic cell accumulation. These results demonstrate that abnormal cell maturation possibly contribute to the development of myopathy and DCM. In conclusion, HOIL-1L is an important intrinsic regulator of cell cycle-related myotube and CM maturation and cell proliferation.

Dilated cardiomyopathy (DCM) is defined by the presence of a dilated ventricle with severe systolic dysfunction, which causes end-stage heart failure¹. The reported prognosis of pediatric DCM patients is extremely poor. Many cases require cardiac transplantation, and the reported 5-year transplantation-free survival rate is only 55–63%^{2,3}. The main evidence-based pharmacological therapies for DCM are digoxin, diuretics, angiotensin-converting enzyme inhibitors, and beta-adrenergic receptor blockers. These drugs improve the prognosis of adult DCM patients^{4,5}; however, it is unclear whether they improve the prognosis of younger patients. One reason for this is that a wide variety of causes and associations have been described for DCM⁶. These pathogenic categories include primary and secondary DCM, and the prognosis depends on them⁷. Therefore, it is important to elucidate the mechanisms underlying each category of DCM to choose appropriate medical therapies.

Regarding progressive severe DCMs, HOIL-1L deficiency was recently reported to be one of the causes of pediatric DCM, and these patients also have myopathy, autoinflammatory syndrome, and pyogenic bacterial diseases⁸. Most HOIL-1L-deficient patients are diagnosed with severe cardiomyopathy until adolescence. Cardiomyopathy is so severe and life-threatening that most of these patients require a heart transplantation in childhood. Unfortunately, heart transplantations are not performed for all patients because of problems including a lack of donor hearts and economic issues. Thus, it is crucial to develop treatments that affect the mechanisms responsible for the development of cardiomyopathy. The mechanisms by which cardiomyopathy develops in HOIL-1L-deficient patients have not been revealed. However, amylopectinosis in skeletal muscle and cardiomyocytes (CMs) of these patients has been identified by autopsy^{8–10}. Amylopectinosis is seen both in Hoil-1l KO mice and HOIL-1L deficient patients, but the phenotype of myopathy and cardiomyopathy is specific to HOIL-1L deficient patients. Because of these facts, the research using human cell line is necessary.

HOIL-1L is a component of the linear ubiquitin chain assembly complex (LUBAC), together with HOIP and SHARPIN. The LUBAC specifically generates a linear ubiquitin chain, which is formed via amino-terminal Met-1-linked ubiquitination^{11–13}. The linear ubiquitin chain plays an important role in mediating NF- κ B activation

¹Department of Pediatrics, Graduate School of Medicine, Kyoto University, 54 Kawahara-cho, Shogoin, Sakyo-ku, Kyoto City, Kyoto 606-8507, Japan. ²Department of Molecular and Cellular Physiology, Graduate School of Medicine, Kyoto University, Yoshidakonoe-cho, Sakyo-ku, Kyoto City, Kyoto 606-8501, Japan. ³Department of Clinical Application, Center for iPS Cell Research and Application (CiRA), Kyoto University, 53 Kawahara-cho, Shogoin, Sakyo-ku, Kyoto City, Kyoto 606-8507, Japan. ✉email: shibaba@kuhp.kyoto-u.ac.jp

and protecting against cell death^{12,13}. Among the three components of the LUBAC, HOIL-1L, especially its UBL domain located in the N-terminal region, is essential for stability of the LUBAC¹⁴ and linear ubiquitination at the TNFR1 signaling complex¹⁵. Furthermore, the RING-IBR-RING (RBR) domain of HOIL-1L modulates immune signaling and cell death via monoubiquitination of the LUBAC¹⁶. These facts shed light on the various clinical phenotypes of HOIL-1L-deficient patients, who also have autoinflammatory syndrome and pyogenic bacterial diseases. However, the mechanisms by which lethal cardiomyopathy develops in these patients have not been elucidated.

Recently, several DCMs were successfully modeled by generating patient-specific human induced pluripotent stem cell (hiPSC)-derived CMs^{17–19}. However, use of hiPSCs to model and study DCM in HOIL-1L-deficient patients has not been reported. Many HOIL-1L-deficient patients are diagnosed with DCM until childhood, and some cases develop DCM in infancy. Almost all HOIL-1L deficient patients have myopathy. Taking these facts into consideration, investigation of human cardiac cell development using hiPSC-derived CMs may be useful to elucidate the mechanism by which DCM develops upon HOIL-1L deficiency, and myoblasts can model the pathophysiology of HOIL-1L deficiency. In this study, we examined the role of HOIL-1L using murine myoblasts and hiPSC-derived CMs to reveal the mechanisms underlying myopathy and cardiomyopathy in HOIL-1L-deficient patients.

Results

Hoil-1l deletion perturbs murine myotube differentiation

To investigate the functions of the mammalian *HOIL-1L* gene in skeletal muscle, we used the murine myoblast cell line C2C12. *Hoil-1l*-KO C2C12 cells were generated using the lenti-CRISPR system. Mutation sites that cause myopathy and severe DCM, which necessitate intensive care of patients, were chosen, and models with KO at two locations, Exon 5 and Exon 7, were generated (Table 1). Exon 5-KO does not conserve the N-terminal domain, while Exon 7-KO does (Fig. 1A, B). HOIL-1L protein is highly preserved between mice and human, and comparison of the amino acid sequence is indicated (Fig. 1A). Amylopectinosis was evaluated by measuring the amount of glycogen in myotubes differentiated from C2C12 cells on day 5 of differentiation in vitro. The amount of glycogen in myotubes differentiated from control, Exon 5-KO, and Exon 7-KO C2C12 cells did not significantly differ. Next, the fusion index and myosin heavy chain (MHC) density, which are indicators of differentiation, were calculated. The fusion index and MHC density on day 5 of differentiation were significantly lower in myotubes differentiated from Exon 5-KO and Exon 7-KO C2C12 cells than in those differentiated from control C2C12 cells (Fig. 1C, Supplementary Fig. 1A). The protein expression level of MHC was also significantly lower in myotubes differentiated from Exon 5-KO and Exon 7-KO C2C12 cells than in those differentiated from control C2C12 cells (Fig. 1D). To assess the impaired phase of myotube differentiation, quantitative PCR (qPCR) was performed to measure the expression levels of the key myogenic transcription factors *Myogenin*, *MyoD*, and *MRF4*. *Myogenin* and *MyoD* expression levels in myotubes differentiated from control, Exon 5-KO, and Exon 7-KO C2C12 cells did not significantly differ during differentiation. However, the expression level of *MRF4*, an early differentiation factor, on days 5 and 6 of differentiation was significantly lower in myotubes differentiated from Exon 5-KO and Exon 7-KO C2C12 cells than in those differentiated from control C2C12

References	Patient	Allele1 (DNA)	Allele2 (DNA)	Allele1 (Protein)	Allele2 (Protein)	Exon	Clinical presentation
Boisson et al	Family 1	c.553C>T	c.ex1_ex4del	Q185*	1–154 del (NTD)	E5/E1-4	Immunodeficiency Autoinflammation Cardiomyopathy
	Family 2	c.121_122delCT	c.121_122delCT	L41fs*7	L41fs*7	E2	
Nilsson et al	Family A	c.1160A>G	c.727G>T	N387S	E243*	E9/E6	Cardiomyopathy
	Family B	c.896-899delAGTG	c.896-899delAGTG	E299Vfs*18	E299Vfs*18	E7	Cardiomyopathy → transplantation
	Family C	c.722delC	c.722delC	A241Gfs*34	A241Gfs*34	E6	Cardiomyopathy
	Family D	c.52G>C	c.52G>C	A18P	A18P	E2	Cardiomyopathy
	Family E	c.ex1_ex4del	c.727_728InsGGCG	1–154 del (NTD)	E243Gfs*114	E1-4/E6	Cardiomyopathy → died of heart failure
	Family F	c.1054C>T	c.1054C>T	R352*	R352*	E9	Cardiomyopathy → transplantation
	Family G	c.817+3_917+4 insG	c.817+3_917+4 insG	R298Rfs*40	R298Rfs*40	E7	Myopathy
	Family H	c.494delG	c.494delG	R165Rfs*111	R165Rfs*111	E5	Cardiomyopathy → transplantation
Krenn et al	Pt 1 and 2	c.896-899delAGTG	c.896-899delAGTG	E299Vfs*18	E299Vfs*18	E7	Cardiomyopathy → die/transplantation

Table 1. Type of mutations and main clinical phenotypes of reported HOIL-1L deficiency families.

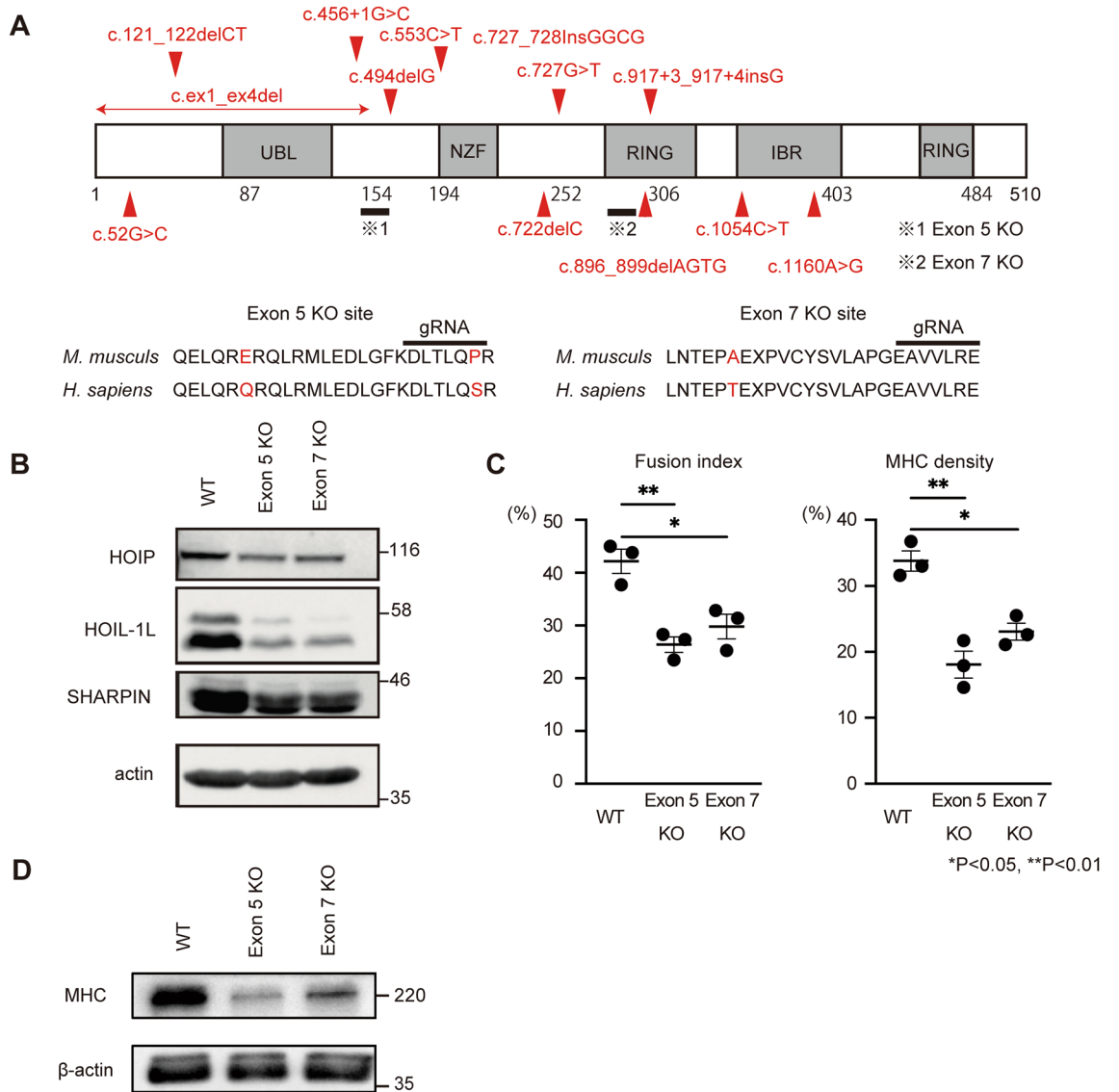


Figure 1. Hoil-11 knockout C2C12 shows impaired myotube differentiation. **(A)** Schematic presentation of reported mutations and Hoil-11 knockout locus of C2C12 myoblast in HOIL-1L protein domains and amino acid sequences near the KO sites. **(B)** Immunoblot analysis of lysates of WT and Hoil-11 knockout myoblasts on day 5. Although HOIP and SHARPIN levels were decreased, HOIL-1L expression level was remarkably decreased in KO C2C12 derived myotubes. **(C)** Fusion index and MHC density were calculated on day 5. All data are presented as mean ± SEM. *P* values from Welch’s *t*-test. WT vs Exon 5 KO and Exon 7 KO. **P*<0.05, ***P*<0.01. **(D)** Western blotting shows impaired expression of MHC in Hoil-11 knockout C2C12 myotube.

cells (Supplementary Fig. 1B). Collectively, these results indicate that Hoil-11 is one of the key factors that affect the early phase of murine myotube maturation. Furthermore, RNA sequencing (RNA seq) was performed of myotubes differentiated from Hoil-11-KO and control C2C12 cells on day 5 of differentiation (Fig. 2A). The expression levels of 396 genes significantly differed by twofold or more between myotubes differentiated from Exon 5-KO C2C12 cells and those differentiated from control C2C12 cells (224 upregulated and 172 downregulated). Among these, expression of genes associated with muscle contraction and muscle structure (*ATP1B2*, *MB*, *TNNC2*, etc.) was significantly higher in myotubes differentiated from control C2C12 cells than in those differentiated from Exon 5-KO C2C12 cells (Fig. 2B). Gene set enrichment analysis (GSEA) and Gene Ontology (GO) analysis showed that the expression of genes linked to processes related to muscle contraction and myogenesis was also decreased in myotubes differentiated from Exon 5-KO C2C12 cells (Fig. 2C–E). Although expression of fewer genes was significantly changed by twofold or more in myotubes differentiated from Exon 7-KO C2C12 cells relative to those differentiated from control C2C12 cells, GSEA and GO analysis yielded the same results as those acquired with myotubes differentiated from Exon 5-KO C2C12 cells. These results indicate that Hoil-11 affects myotube differentiation regardless of deficient domain.

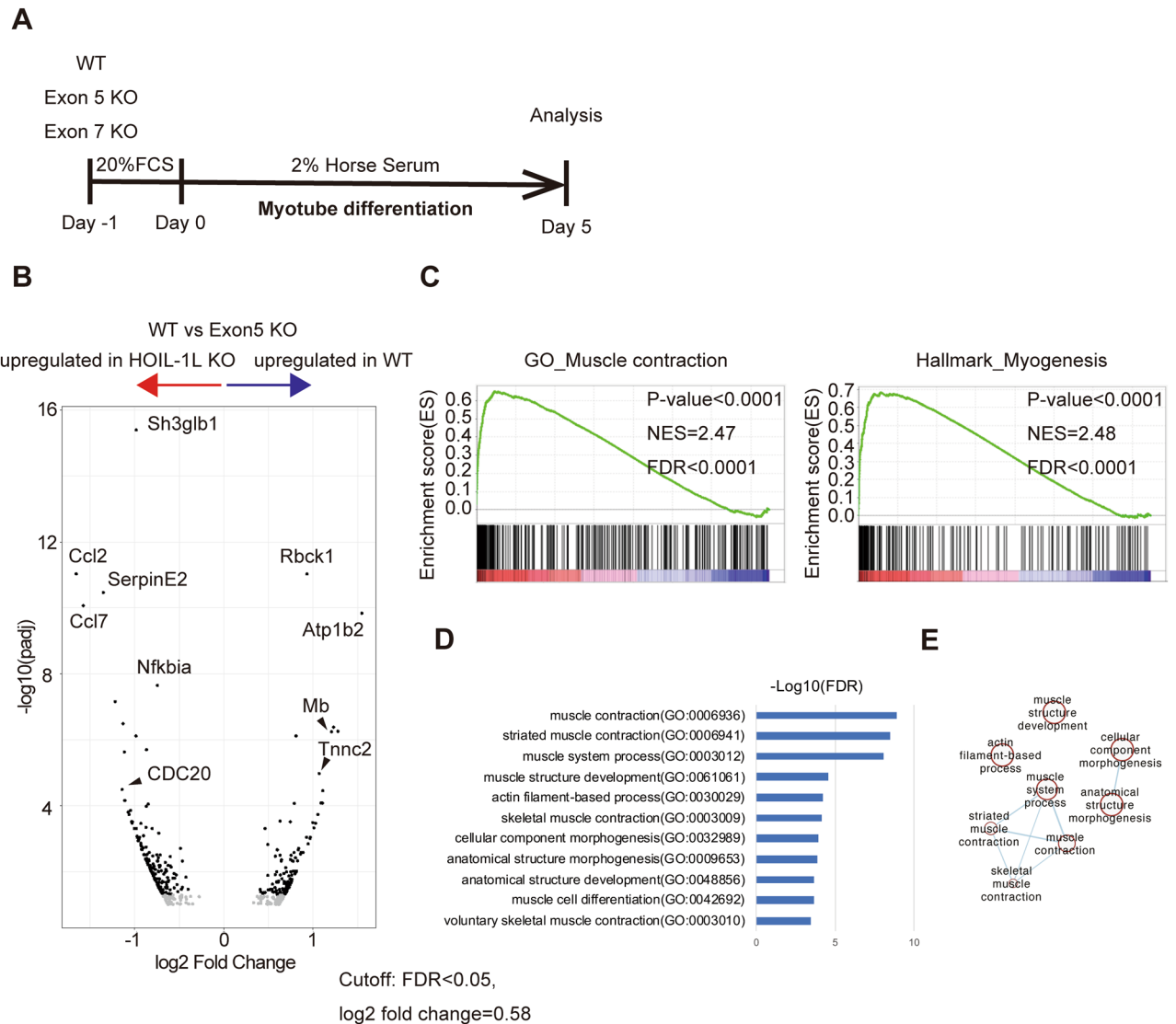


Figure 2. RNA-seq analysis of Hoil-1l KO C2C12 shows supportive data to impaired myotube differentiation. (A) A scheme of myotube differentiation protocol of C2C12 myoblast. Myoblasts were cultured with DMEM containing 20% serum for 24 h. On day 0, the medium was replaced to DMEM containing 2% horse serum and myoblasts were cultured for next 5 days for RNA-seq analyses. (B) Distribution of \log_2 fold change between Hoil-1l Exon5 KO C2C12 myotubes and WT C2C12 myotubes versus the adjusted *P*-value (FDR). By setting the FDR cutoff as 0.1, 172 genes were upregulated in WT C2C12 myotubes and 224 genes were upregulated in Hoil-1l KO C2C12 myotubes. Genes associated with skeletal muscle function such as ATP1B2, MB and TNNC2 were down-regulated in Hoil-1l KO C2C12 myotubes. (C) GSEA identified a significant enrichment of gene set associated with muscle contraction and myogenesis in WT C2C12 myotubes. (D) The enrichment analysis by g:Profiler also showed significant enrichment of gene sets associated with muscle contraction and morphogenesis. (E) Pathway enrichment analysis results are visualized in Cytoscape.

Hoil-1l deletion alters the cell cycle according to RNA seq analysis of C2C12 myoblasts

Further GSEA revealed that genes associated with the G2M checkpoint and mitotic spindle formation were significantly upregulated in myotubes differentiated from Hoil-1l-KO C2C12 cells (Fig. 3A). Consistently, significantly more myoblasts were positively stained for phosphorylated (Ser10) histone H3, a marker of mitotic cells, in myotubes differentiated from Hoil-1l-KO C2C12 cells than in those differentiated from control C2C12 cells (Fig. 3B). *CDK1*, *AURKB*, *CDC20*, and *CCNB2*, which are involved in M phase of the cell cycle, were significantly upregulated in myotubes differentiated from Hoil-1l-KO C2C12 cells (Fig. 3C). These results suggest that cell cycle alterations induced by Hoil-1l deletion impair myotube differentiation.

Clinical history of a HOIL-1L-deficient patient and hiPSC production

From the results so far, we predicted that cell cycle alteration probably occurs also in HOIL-1L deficient cardiomyocyte. Next, we focused on the effect of HOIL-1L on CMs using hiPSCs. We generated hiPSCs from a HOIL-1L-deficient patient and two unrelated healthy control volunteers. Two hiPSC clones were established from the

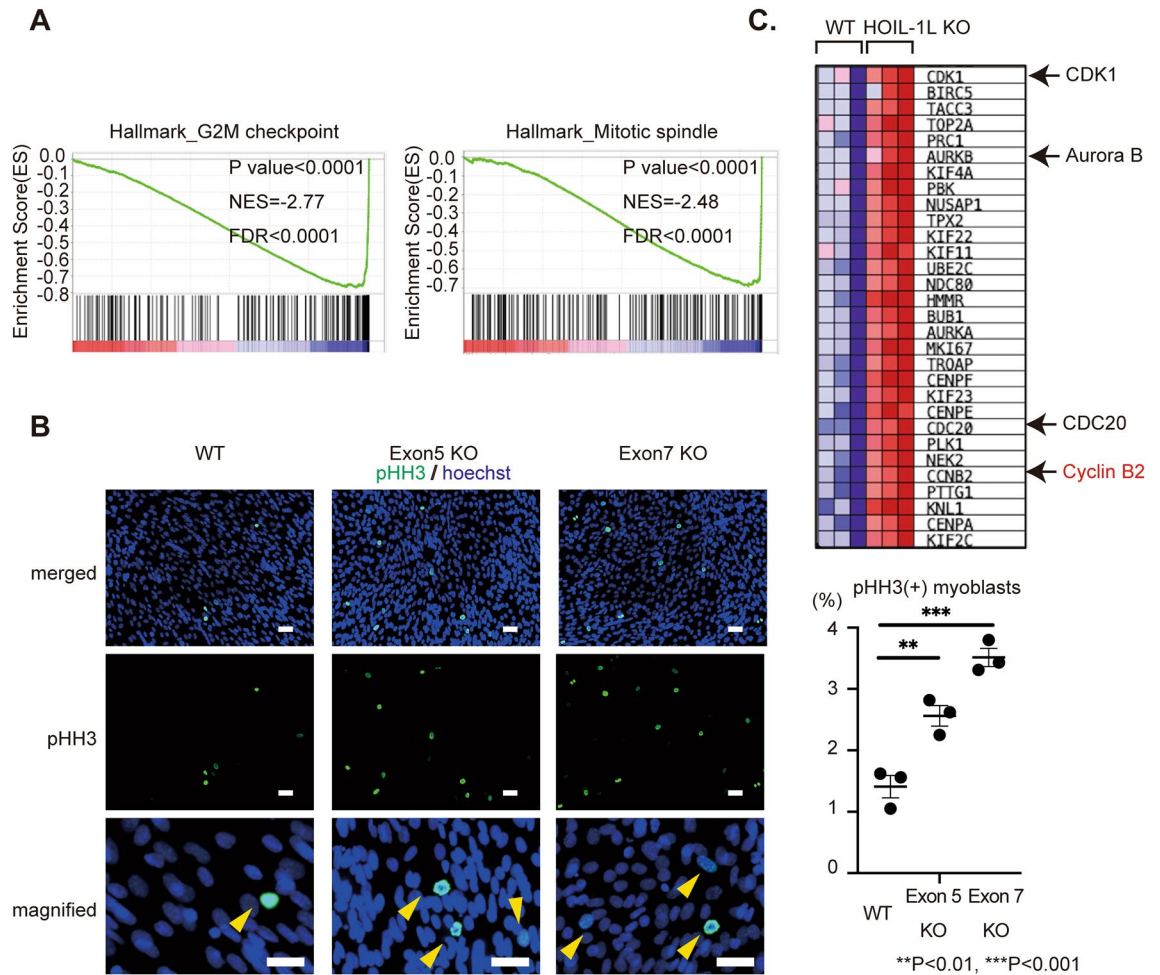


Figure 3. RNA-seq analysis of Hoil-1L KO C2C12 shows mitotic accumulation in Hoil-1L KO C2C12 myotubes. (A) GSEA identified a significant enrichment of gene set associated with G2M checkpoint and mitotic spindle in Hoil-1L KO C2C12 myotubes. (B) Immunostaining of histone H3 phosphorylation (pHH3) of C2C12 myotubes showed more PHH3 positive Hoil-1L KO C2C12 myoblasts. From top to bottom, they are merged, pHH3 signal only and magnified images, respectively. Bar = 50 μ m. (N = 3 independent experiments, All data are presented as mean \pm SEM. *P* values from Welch's *t*-test. WT vs Exon5 KO and Exon7 KO. ***P* < 0.01, ****P* < 0.001). (C) Heatmaps of the G2M check point associated genes enriched in Hoil-1L KO C2C12 myotubes compared with WT C2C12 myotubes. Especially, CDK1, AURKB, CDC20 and CCNB2 (noted with red color; cyclin family), which promote entry into mitosis and maintain of the mitosis state.

HOIL-1L-deficient patient. This patient was diagnosed with a homozygous missense mutation, a substitution of leucine for proline at residue 114 (L114P), by whole genome sequencing. The sequence was confirmed by Sanger sequencing (Supplementary Fig. 2A). She had an autoinflammatory syndrome, pyogenic bacterial diseases, and frequent ventricular arrhythmia with elevation of type-B natriuretic peptide (BNP), which possibly implied an initial presentation of heart failure. In infancy, she began to suffer from recurrent episodes of fever with lymphadenopathy. Based on laboratory examinations, she was diagnosed with IgA deficiency at 2 years old and with IgG2 and IgG4 deficiency at 5 years old. During early childhood, she often suffered from bacterial pneumonia and otitis media, and from fever associated with lymphadenopathy and inflammatory bowel disease. In the second decade of life, she was diagnosed with epilepsy based on myoclonus seizures and spike-and-wave on an electroencephalogram, and she needed antiepileptic drugs to control the seizures. In the third decade of life, she developed a walking difficulty due to mild myopathy and palpitations due to ventricular arrhythmia in more than 15% of total heart beats. Furthermore, echocardiography showed a mildly/moderately reduced left ventricular ejection fraction (51%) and a thin left ventricular wall with an elevated BNP level. She died in young adulthood because of these complications. Her elder sister, who possibly had the same mutation, was diagnosed with DCM and also died of heart failure in young adulthood. After performing pluripotency marker analysis by immunohistochemistry (Supplementary Fig. 2B) and confirming that full-length HOIL-1L was not expressed in hiPSCs derived from the patient by western blotting (Supplementary Fig. 2C), these hiPSCs were differentiated into CMs (hiPSC-CMs) and purified by glucose deprivation.

Amylopectinosis was not detected in HOIL-1L-deficient hiPSC-CMs

To determine if the clinical features could be mimicked in patient-specific hiPSC-CMs (HOIL-1L hiPSC-CMs), amylopectinosis in the cytoplasm was evaluated by Periodic acid-Schiff (PAS) staining. All HOIL-1L and control hiPSC-CMs exhibited PAS-positive staining in their cytoplasm. However, this disappeared upon digestion with amylase in both HOIL-1L and control hiPSC-CMs. The glycogen level was not significantly higher in HOIL-1L hiPSC-CMs than in control hiPSC-CMs. (Supplementary Fig. 2D, E). These results indicate that amylopectinosis cannot be reproduced in HOIL-1L hiPSC-CMs using a short period of in vitro differentiation and a culture protocol.

HOIL-1L hiPSC-CMs are large and multinucleated

HOIL-1L hiPSC-CMs were significantly larger than control hiPSC-CMs. HOIL-1L hiPSC-CMs were more multinucleated than control hiPSC-CMs (Fig. 4A, B). RT-qPCR revealed that expression of *MYH7*, a cardiomyogenesis-related gene, was higher in HOIL-1L hiPSC-CMs than in control hiPSC-CMs (Supplementary Fig. 3A). Based on these results, we hypothesized that HOIL-1L deficiency caused cytokinesis failure during cardiomyogenesis. In immunohistochemical analysis, significantly more HOIL-1L hiPSC-CMs than control hiPSC-CMs were positively stained with phosphorylated (Ser10) histone H3, a marker of mitotic cells (Fig. 4C, D). Furthermore, the ratio of Ki67 positive CMs is significantly lower in HOIL-1L hiPSC-CMs than in control hiPSC-CMs (Supplementary Fig. 3B). Considering that the results of pHH3 immunostaining indicate cell cycle arrest at M phase in HOIL-1L hiPSC-CMs, the decrease of Ki67 positive CMs is reasonable, and the results possibly indicate deterioration of cell proliferation ability in HOIL-1L hiPSC-CMs. In other words, HOIL-1L deletion possibly leads to abnormal cell cycle patterns in CMs and thereby causes excessive accumulation of these cells in M phase, resulting in production of larger CMs with more multinucleation. Next, we focused on the finding that expression of *SERPINE2* was significantly higher in myotubes differentiated from Hoil-1l-KO C2C12 cells based on RNA seq. *SERPINE2* is reportedly associated with cardiac fibrosis²⁰. In qPCR analysis, *SERPINE2* expression was significantly higher in HOIL-1L hiPSC-CMs than in control hiPSC-CMs when vimentin (*VIM*), a cardiac fibroblast gene, was used to standardize gene expression, but not *GAPDH* and cardiac troponin T (*TNNT2*) (Supplementary Fig. 3C). As it has been reported that mitotic catastrophe in cardiomyocyte causes cardiac fibrosis and cell death²¹, the effect of M phase accumulation and upregulated *SERPINE2* expression in hiPSC-CMs was evaluated by TUNEL staining. A significantly higher percentage of HOIL-1L hiPSC-CMs than control hiPSC-CMs was TUNEL-positive (Fig. 5A, B). These results indicate that accumulation in M phase causes death of CMs and that upregulated *SERPINE2* expression in cardiac fibroblasts may cause paracrine fibrogenesis in differentiated CMs (Fig. 5C).

Heart development is perturbed in Hoil-1l-KO mouse embryos

To assess heart development in vivo, we investigated control and Hoil-1l-KO mouse embryos, which were generated previously¹⁴. H&E staining of E10.5 normal and Hoil-1l null/+ mouse embryos was performed. In normal embryos, the embryonic atrium and ventricle began to undergo septation to produce the four chambers. On the other hand, in Hoil-1l null/+ embryos, the heart began to form a round structure via ballooning. It was difficult to discriminate the atrium and ventricle during this period (Supplementary Fig. 4). These results indicate that Hoil-1l KO causes embryonic stunting including severe heart development delay.

Discussion

DCM is a leading cause of heart failure, and the prognosis is poor. Heart transplantation is indicated for patients with end-stage DCM, but not all patients can undergo this procedure. While genetic alterations affect sarcomeric proteins and contractile function in some DCM cases, HOIL-1L deficiency is reportedly a novel cause of severe DCM. Mechanistic insight into this may help to develop a new treatment. For this purpose, development of hiPSC-CMs and the role of Hoil-1l in murine myoblasts were investigated in this study. Our results obtained using hiPSC-CMs and murine myoblasts indicate that cell cycle abnormalities probably contribute to the development of DCM in HOIL-1L-deficient patients.

In this study, we used patient-specific hiPSCs because recent advances in hiPSC technologies have made it possible to model genetic heart disease in vitro. Differentiated hiPSC-CMs could be purified to around 80–90% CMs, including atrial and ventricular cells, in experiments of cardiac differentiation. However, other populations such as cardiac fibroblasts are contained. Therefore, a homogeneous population, the murine myoblast C2C12 cell line, was also used as a model of HOIL-1L myopathy, and this model showed the same phenotypes as HOIL-1L hiPSC-CMs. We performed experiments using both hiPSC-CMs and myotubes differentiated from C2C12 cells to focus not only on myopathy but also on cardiomyopathy. Lastly, all the data was gathered to analyze and discuss the disease mechanisms.

Amylopectinosis, an amylopectin-like polysaccharide, is observed in both skeletal and cardiac muscles in genetic diseases associated with glycogen metabolism²². Amylopectinosis was detected by biopsy and autopsy of HOIL-1L-deficient patients^{8–10,23}. However, we could not reproduce amylopectinosis in HOIL-1L hiPSC-CMs or myotubes differentiated from Hoil-1l-KO C2C12 cells. hiPSC-CMs reportedly exhibit metabolically immature phenotypes. These findings are expected because the main energy source is glycolytic metabolism in hiPSC-CMs but oxidative phosphorylation in matured CMs²⁴. Much longer culture and a more biogenic culture condition is presumably required to reproduce amylopectinosis.

C2C12 myoblasts spontaneously differentiate into myotubes upon differentiation in a medium containing of 2% horse serum for 5–7 days, but myotubes do not exhibit spontaneous contraction during this differentiation. These facts are probably associated with our finding that amylopectinosis could not be reproduced. Thus, the effect of amylopectinosis in HOIL-1L-deficient patients remains unclear. If novel myocyte and CM differentiation

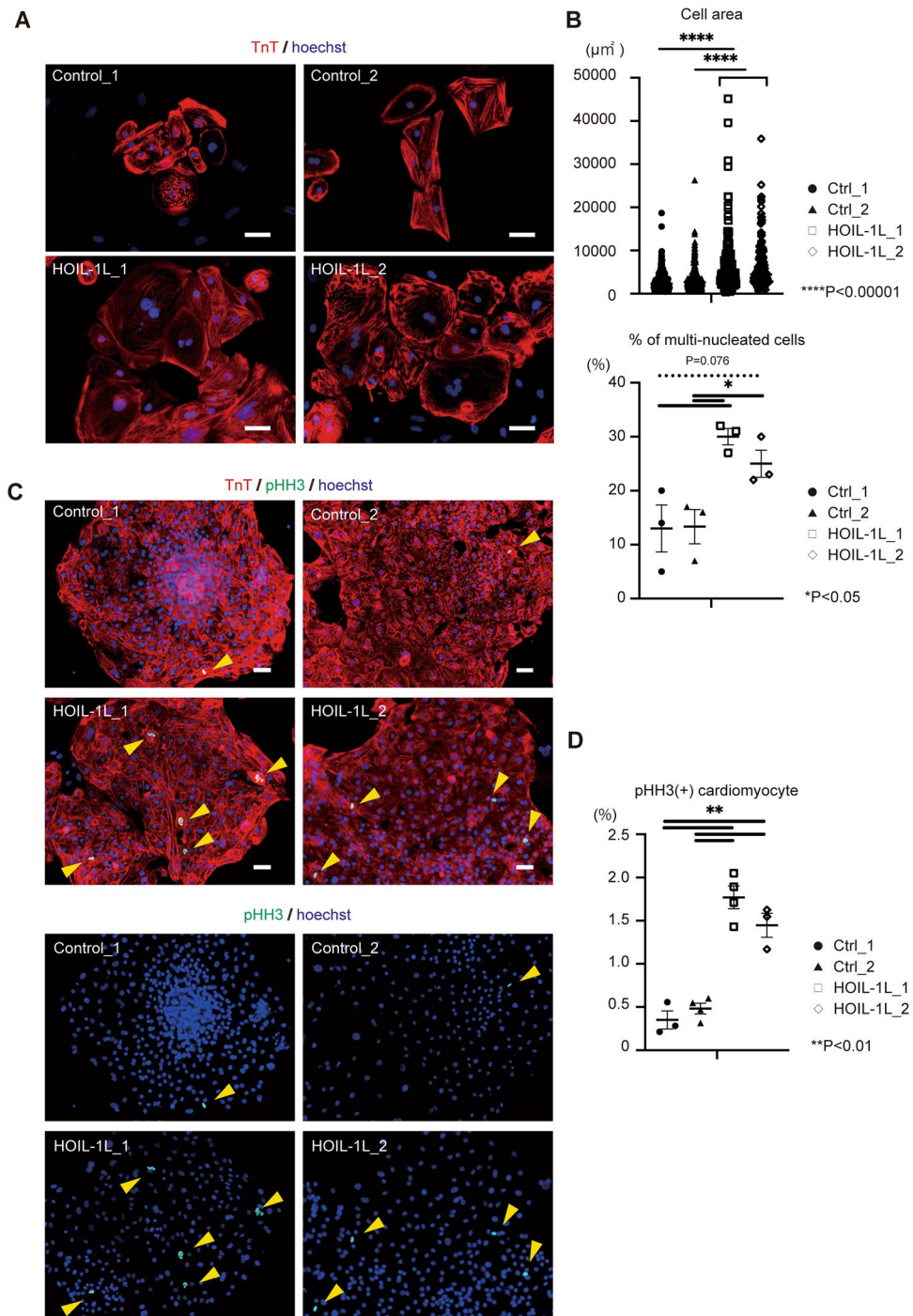


Figure 4. Phenotype of HOIL-1L deficient patient-specific hiPSC-CMs. **(A)** Representative images of immunostaining for cardiac troponin T (cTnT). The patient hiPSC derived hiPSC derived CMs showed larger size and multi-nucleation compared with control hiPSC derived CMs. Bar = 50 μm . **(B)** Quantification of cell size and multi-nucleation in control and HOIL-1L deficiency patient iPSC derived CMs. (> different 3 passages and $n > 200$, **** $P < 0.00001$, * $P < 0.05$). **(C)** Immunostaining of histone H3 phosphorylation (pHH3) of hiPSC-CM showed more pHH3 positive hiPSC-CMs of HOIL-1L deficiency hiPSC-CMs than control hiPSC-CMs. From top to bottom, they are merged and pHH3 signal only images, respectively. Bar = 50 μm . **(D)** Quantification of pHH3 + hiPSC-CMs showed significantly higher ratio in HOIL-1L deficiency hiPSC-CMs than control hiPSC-CMs. (> different 3 passages, ** $P < 0.01$). All data are presented as mean \pm SEM. P values from Welch's t -test.

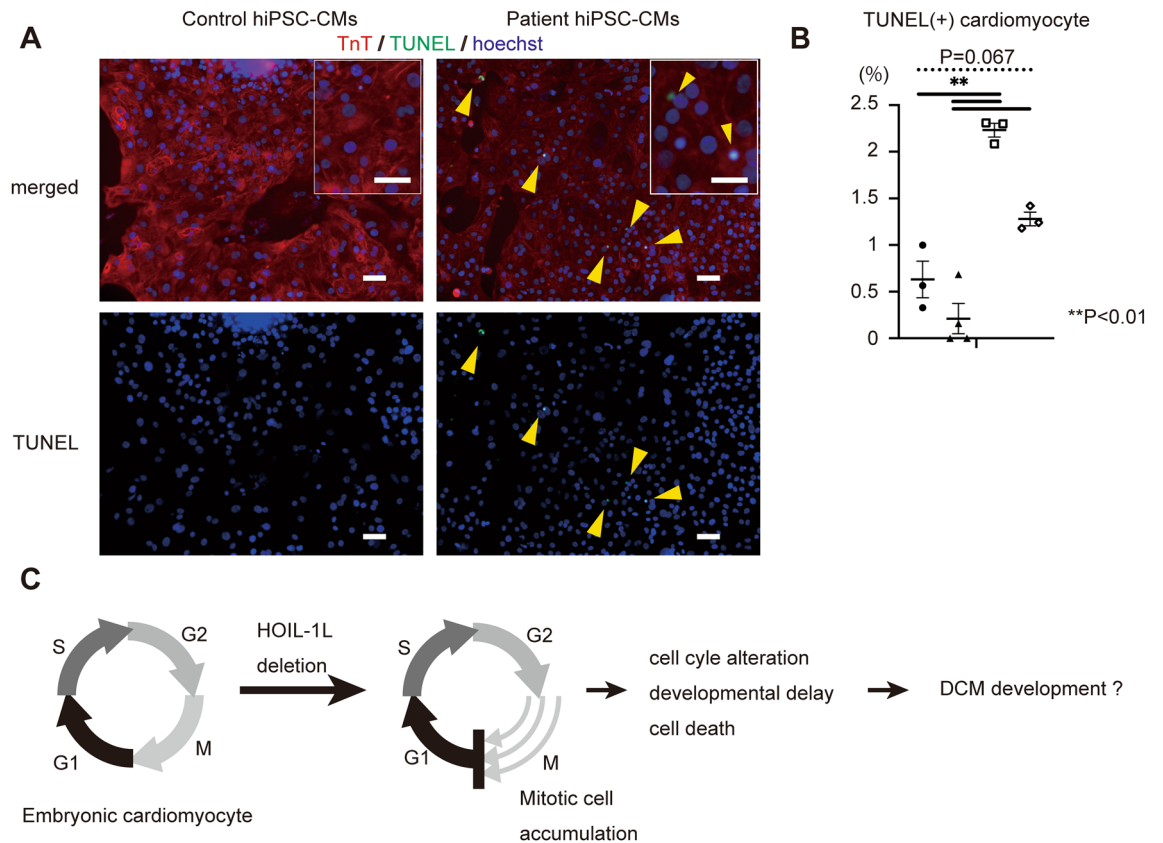


Figure 5. TUNEL assay in hiPSC-CMs and predictive mechanism of dilated cardiomyopathy development in HOIL-1L deficiency. (A) Representative data of TUNEL staining of HOIL-1L deficiency hiPSC-CMs and control hiPSC-CMs. From top to bottom, they are merged and TUNEL signal only images, respectively. Bar = 50 μ m. (B) The ratio of TUNEL positive hiPSC-CMs was significantly higher in HOIL-1L deficiency compared to control. (> different 3 passages, ** $P < 0.01$). (C) Predictive mechanism of dilated cardiomyopathy development in HOIL-1L deficiency. All data are presented as mean \pm SEM. P values from Welch's t -test.

protocols that mimic the long lifespans of mice and humans are developed, the effect of amylopectinosis on cardiomyopathy and myopathy will hopefully be revealed by in vitro experiments.

HOIL-1L hiPSC-CMs were morphologically abnormal, and differentiation of myotubes from Hoil-11-KO C2C12 cells was impaired. These results imply that abnormalities in the maturation of CMs and skeletal muscle are related to the pathophysiology of DCM and myopathy in HOIL-1L-deficient patients. Hypertrophic vacuolar cardiomyopathy was reported to be a pathological finding in autopsies of HOIL-1L-deficient patients²³, and this is probably associated with impaired differentiation of CMs and development of DCM.

RNA seq revealed that expression of genes associated with muscle contraction and muscle structure was significantly lower in myotubes differentiated from Hoil-11-KO C2C12 cells than in those differentiated from control C2C12 cells. This result supports our speculation.

Furthermore, GSEA detected increased expression of genes associated with mitosis regulation. *CCNB2*, which encodes a member of the cyclin family, was upregulated in myotubes differentiated from Hoil-11-KO C2C12 cells. Members of the cyclin family play important roles in cell cycle control in CMs; therefore, HOIL-1L deletion was predicted to affect the cell cycle in CMs. To determine whether the cell cycle was abnormal in hiPSC-CMs, a mitotic cell marker was evaluated. This revealed that HOIL-1L hiPSC-CMs abnormally accumulated in M phase. During embryogenesis and fetal development of the mammalian heart, development of the cardiac chambers and further growth of the heart are accomplished by hyperplastic growth of CMs in the cell cycle. After birth, CMs exit the cell cycle and stop proliferating²⁵. Abrogation of the cell cycle results in multinucleation and polyploidy in CMs²⁶. Cell cycle alteration during late embryonic development due to loss of cytokinesis regulators (e.g., *GAS2L3*) leads to premature binucleation of CMs. *GAS2L3* is required for mitosis of CMs around the late embryonic and early postnatal stages. Mice with loss of *GAS2L3* exhibit compensatory CM hypertrophy, and this change is associated with interstitial fibrosis, ventricular dilation, and contractile dysfunction, resulting in early death of mice²⁷. Mitotic catastrophe, namely, mitotic cell accumulation, causes cell death and DCM²¹. In patients with HOIL-1L deletion, CM hypertrophy, interstitial fibrosis, and ventricular dilation have been reported^{8–10,23}, and these changes are thought to occur due to cell cycle alteration, accumulation of CMs in M phase, and eventually cell death. Recently, it was reported that LUBAC had a novel function in chromosome alignment and segregation. Interestingly, LUBAC mediated the promotion of CENP-E, kinetochore motor, attachment to kinetochores by linker ubiquitination^{28,29}. Thus, the suppression of LUBAC causes a prolonged mitotic delay, chromosome missegregation during anaphase and increased mitotic cell death. The same result was revealed in our study, so

further experiments are needed to show the relationship between cell cycle alteration in cardiomyocytes and the development of DCM in HOIL-1L deficiency.

The LUBAC is a trimer of HOIL-1L, SHARPIN, and HOIP, and has various functions such as in cell death and carcinogenesis. Cardiomyopathy and myopathy have been observed only in HOIL-1L-deficient patients; therefore, it is unlikely that SHARPIN, HOIP, and the LUBAC are also involved in these pathologies.

Findings from our study provide the first evidence for cell cycle alteration in HOIL-1L deficiency. This abnormality may lead cell death in cardiomyocytes and causes development of DCM in HOIL-1L deficiency patients. These findings are compatible to clinical phenotype. However, we could not reveal more detailed mechanisms of HOIL-1L cell cycle regulation and relationship between cell cycle alteration and cell death. Further studies in vitro/vivo by more detailed methods are needed by using more purified CMs or other populations, such as cardiac fibroblasts.

In conclusion, hypertrophic change of CMs observed at autopsy in HOIL-1L-deficient patients and developmental delay of the heart in *Hoil-1l*-KO mice were reproduced using HOIL-1L hiPSC-CMs, and cell cycle alteration was possibly indicated to be one of the causes of these abnormalities. In addition, cell death, e.g. apoptosis, occurring after accumulation of CMs in M phase contribute to the onset and progression of DCM in HOIL-1L-deficient patients. Based on all these results, we conclude that HOIL-1L affects the development of myopathy and DCM. Our results will help to develop new treatments for lethal DCM in HOIL-1L-deficient patients.

Materials and methods

hiPSC culture

hiPSCs were generated from an Asian female HOIL-1L-deficient patient and healthy controls and kindly donated by the Center for iPS Cell Research and Application (Kyoto University, Kyoto, Japan). Patient-specific (HOIL-1L_1, CiRA-j-0154B and HOIL-1L_2, CiRA-j-0154D) and healthy control hiPSCs (Control_1, CiRA-j-1616-A, Asian female volunteer) were established from the peripheral blood mononuclear cells (PBMCs) using episomal vectors containing reprogramming factors³⁰. Another control hiPSC line from Asian male (Control_2, 110F5) was established as described previously³¹. Each cell line stored in liquid nitrogen using STEM-CELLBANKER (Takara, Cat.# 11924) and once thawed in 37 °C water bath, it was maintained in mTeSR1 medium (Stem Technologies, Cat.# 85,850) as previously reported³². Each cell was stocked at less than 15 passages, and all experimentations were done between 20 and 45 passages. The sequence of RBCK1 gene was confirmed by Sanger sequencing at the beginning of key experiments. Pluripotency of CiRA-j-1616-A, CiRA-j-0154B and CiRA-j-0154D was evaluated by OCT3/4 and NANOG mRNA expression by TaqMan qPCR and pluripotency of control_2 was evaluated by quantitative PCR analysis of *Oct 3/4*, *Sox2*, *Klf4*, and *c-Myc* using SYBR green. Cells were passaged every 4–5 days at 1:10 or 1:12 ratio using accutase (Nacalai Tesque, Cat.# 12679-54). Dissociated cells were seeded on Matrigel-coated 6-well plates. The medium was supplemented with 5 µM Y27632 (TOCRIS, Cat.# 1254), a Rho-associated kinase inhibitor, on the first day of each passage. All cell lines were authenticated by their name, checked their sterility regularly, and monitored of mycoplasma contamination using by PCR kit (Minerva biolabs, Cat.# 11-9025).

CM differentiation from hiPSCs

CMs were differentiated from hiPSCs using a previously reported protocol³³. Briefly, hiPSCs were seeded into a 12-well growth-factor-reduced (GFR) Matrigel-coated plate, grown for 4 days at 37 °C in 5% CO₂ and mTeSR1 medium, and allowed to reach 80–90% confluency. On day 0 of differentiation, the medium was changed to differentiation media, which was RPMI containing 2% B27 minus insulin supplement (Gibco, Cat.# A18956-01) and 10–12 µM CHIR99021 (Selleck, Cat.# S2924), a GSK3 inhibitor. After incubation for 24 h, the medium was replaced with fresh differentiation medium. On day 3, the medium was replaced with differentiation medium containing 5 µM IWP-2 (TOCRIS, Cat.# 3533), a Wnt inhibitor. On day 5, the medium was replaced with fresh differentiation medium. On day 7, B27 minus insulin was replaced with a B27 supplement (Gibco, Cat.# 17504044). Differentiated hiPSC-CMs were purified in glucose-depleted lactate medium as described previously³⁴.

C2C12 cell culture

C2C12 cells were kindly provided by Dr. Yuji Yamanashi (The Institute of Medical Science, The University of Tokyo)³⁵. The growth medium was DMEM/F12 (Sigma-Aldrich, Cat.# D6421) containing 20% FBS, 2 mM glutamine (Gibco, Cat.# 25030081), 100 units/mL penicillin, and 100 µg/mL streptomycin. Cells were incubated at 37 °C in a humidified incubator containing 5% CO₂. Myoblasts were differentiated into myotubes in DMEM/F12 medium containing 2% horse serum (Gibco, Cat.# 16050122, Lot. 1968945)^{36,37}.

Generation of *Hoil-1l*-KO C2C12 cells

Lenti-CRISPR v2 (Addgene, Cat.# 52961), which contains a puromycin resistance gene, carrying a guide RNA oligonucleotide (5'-acctcacccttcagtcacgg-3' for Exon 5 of the *Hoil-1l* gene or 5'-acgcagcaccacggcctcgc-3' for Exon 7 of the *Hoil-1l* gene) was constructed. HEK293T cells were transfected with the plasmids using Lipofectamine 2000 (Thermo Fisher, Cat.# 11668019). Viruses were harvested at 48 h after transfection, and the media were filtered through a 0.45 µm PES filter. C2C12 cells were transduced with the viruses in medium containing 10 µg/mL polybrene. At 24 h after transduction, puromycin selection was started. The selected cells were collected and KO of *Hoil-1l* was confirmed by Sanger DNA sequencing.

Immunohistochemistry and TUNEL assay

Myotubes differentiated from C2C12 cells on day 5 of differentiation were fixed in 4% paraformaldehyde (PFA) for 1 h at 4 °C, permeabilized in 0.1% Triton X-100 for 10 min at room temperature, and blocked in PBS

containing 3% skim milk for 1 h. Thereafter, myotubes were stained with an anti-MHC antibody (1:200, mouse monoclonal, R&D Systems, Cat.# MAB4470). The fusion index was calculated by dividing the number of nuclei in myotubes by the total number of nuclei in a field of view³⁶. The MHC density was calculated by dividing the area occupied by MHC-positive myotubes by the total area of the field of view. The fusion index and MHC density were reported as averages of at least three fields of view (> 500 total nuclei). Three independent experiments were performed for the calculation. For pluripotency marker analysis, undifferentiated hiPSC colonies were fixed in the same way, and fixed cells were stained with mouse anti-Oct3/4 (1:50, Santa Cruz Biotechnology, Cat.# sc5279) and anti-TRA1-81 (1:100, Millipore, Cat.# MAB4381) antibodies. Cells were then incubated with Alexa Fluor-conjugated secondary antibodies (1:1000) overnight at 4 °C. Nuclei were stained with Hoechst 33342 (1:1000, Invitrogen, Cat.#H3570). For immunofluorescence microscopy analysis of hiPSC-CMs, size and multinucleation were analyzed after around 50–60 days of differentiation and mitosis was analyzed after 20 days of differentiation. hiPSC-CMs were replated onto GFR Matrigel-coated 24-well dishes, incubated at 37 °C in 5% CO₂ for 72 h, fixed in 4% PFA for 1 h at 4 °C, permeabilized in 0.1% Triton X-100 for 10 min at room temperature, and blocked in PBS containing 3% skim milk for 1 h. Thereafter, hiPSC-CMs were stained with anti-cTnT (1:100, mouse monoclonal, Thermo Fisher, Cat.# MA5-12960) and anti-phospho-histone H3 (Ser10) (1:1000, rabbit monoclonal, Cell Signaling, Cat.# D7N8E) antibodies. After primary antibody treatment, cells were rinsed three times with PBS for 5 min at room temperature and then incubated overnight at 4 °C with secondary antibodies diluted 1:1000 in PBS. Nuclei were stained with Hoechst 33342. For isotype controls, mouse IgG1 isotype (BD Biosciences, Cat.# 554121) and rabbit IgG isotype (BD Biosciences, Cat.# 550875) were used. All immunofluorescence analyses were performed using a BZ-710X microscope (Keyence). The TUNEL assay was performed using a Cell Death Detection Kit (Roche, Cat.# 11684795910) following the manufacturer's protocol.

Western blotting

Myotubes at day 5 of differentiation were lysed in M-PER buffer (Thermo Scientific, Cat.# 78501) containing 1 × protease inhibitor and then incubated on ice. The samples were sonicated on ice for 30 s. The lysates were incubated on ice for 10 min and then centrifuged at 15,000 rpm for 15 min. Protein concentrations were determined using the Bradford assay. Thereafter, 30 µg of protein was loaded onto each lane of 10% SDS-PAGE gels. The membranes were probed with an anti-MHC antibody (1:100, R&D Systems, Cat.# MAB4470) in blocking buffer (5% BSA) at 4 °C overnight, washed, incubated in secondary antibodies for 1 h at room temperature, developed using ECL western blotting substrate (Bio-Rad, Cat.# 1705060), and imaged using the ChemiDoc MP Imaging System (Bio-Rad). The blots were cut prior to hybridization with antibodies, and two replicates were done at the same time for Fig. 1B and Supplementary Fig. 2C as shown in supplementary Fig. 5.

Flow cytometry

hiPSC-CMs were dissociated on the day of evaluation by incubating them in 0.25% trypsin–EDTA for 10–15 min at 37 °C. They were fixed in Cytofix/Cytoperm solution (BD Biosciences, Cat.# 554714) for 20 min at 4 °C, washed with BD Perm/Wash buffer (Cat.# 554723), stained with an anti-cTnT antibody (1:200, mouse monoclonal, Thermo Fisher, Cat.# MA5-12960) followed by Alexa Fluor-conjugated secondary antibodies, and analyzed using FACSverse (BD Biosciences). In cell cycle analysis, hiPSC-CMs after 20 days of differentiation were gathered. After fixing and washing the hiPSC-CMs as described above, they were stained with an anti-cTnT antibody (1:200) and an anti-Ki67 antibody (1:400, rabbit monoclonal, Cell Signaling Technology, Cat.# 9129) followed by Alexa Fluor-conjugated secondary antibodies, and analyzed using FACSverse. Data were collected from at least 10,000 events. Data with > 70% cTnT populations were used for all experimental analyses.

qPCR analysis of C2C12 cell-derived myotubes and hiPSC-CMs

Total RNA was extracted from day 0 to day 7 of myotube differentiation using an RNeasy Mini Kit (Qiagen, Cat.# 74104) according to the manufacturer's instructions. qPCR was performed using SYBR Green PCR Master Mix (Takara, Cat.# RR820) on a StepOnePlus system (Thermo Fisher Scientific) with the $\Delta\Delta C_t$ method. GAPDH was used to standardize gene expression. Total RNA was extracted from hiPSC-CMs at 45–60 days after differentiation.

H&E staining

Hoil-11-KO and control mouse embryos were generated as described previously¹⁴. Paraffin sections of E10.5 Hoil-11 null/+ and control littermate mouse embryos were deparaffinized and stained with H&E.

RNA seq

RNA was isolated from C2C12 cells using a RNeasy Mini Kit, according to the manufacturer's instructions. RNA integrity was measured using an Agilent 2200 TapeStation and RNA Screen Tapes (Agilent Technologies). Sequencing libraries were prepared using a NEBNext Ultra II RNA Library Kit for Illumina (New England Biolabs) with the NEBNext Poly (A) mRNA Magnetic Isolation Module (New England Biolabs), according to the manufacturer's protocol. Prepared libraries were run on an Illumina HiSeq X sequencing platform in 150 bp paired-end mode. Sequencing reads were aligned to the GRCh38 mouse genome assembly using STAR (c.2.5.3). Mapped reads were counted for each gene using the GenomonExpression pipeline (<https://github.com/Genomon-Project/GenomonExpression>). Normalization of the read counts of RNA seq data and differential expression analysis were performed using the Bioconductor package DESeq2 (version 1.26.0). Differentially expressed genes with a greater than twofold change and a false discovery rate less than 0.1 were filtered and evaluated. RNA seq data have been deposited with links to BioProject accession number PRJDB17426 in the DDBJ BioProject database.

GSEA

GSEA was performed using software (version 4.0.3) from the Broad Institute. Normalized expression data obtained from RNA seq were assessed using GSEA software and the Molecular Signature Database (<http://www.broad.mit.edu/gsea/>). c5 ontology gene sets were used, and a false discovery rate less than 0.01 was considered to be statistically significant. Pathway enrichment analysis using g:Profiler and visualization of enrichment results in an enrichment map were performed using Cytoscape software (version 3.7.2) as described previously³⁸.

Statistical analysis

Data are shown as mean ± SEMs, as indicated in the figure legends. All statistical analyses were performed using Welch's *t*-test with GraphPad Prism (version 9.00, GraphPad Software). *P* < 0.05 was defined as significant.

Ethical statement

Use of patient-derived iPSCs was approved by the Ethics Committee of Kyoto University (R0091 and G0687), and written informed consent obtained from the donor (or their guardians) in accordance with the Declaration of Helsinki.

Data availability

All data presented in this study are available in the main text, in Supplemental items file, and from the corresponding author upon request.

Received: 3 December 2023; Accepted: 19 March 2024

Published online: 17 April 2024

References

- Lipshultz, S. E. *et al.* Cardiomyopathy in children: classification and diagnosis—A scientific statement from the American Heart Association. *Circulation* **140**, e9–e68. <https://doi.org/10.1161/CIR.0000000000000682> (2019).
- Daubeney, P. E. *et al.* Clinical features and outcomes of childhood dilated cardiomyopathy: Results from a national population-based study. *Circulation* **114**, 2671–2678. <https://doi.org/10.1161/CIRCULATIONAHA.106.635128> (2006).
- Dzau, V. J. *et al.* Sustained effectiveness of converting-enzyme inhibition in patients with severe congestive heart failure. *N. Engl. J. Med.* **302**, 1373–1379. <https://doi.org/10.1056/NEJM198006193022501> (1980).
- Yusuf, S. *et al.* Effect of enalapril on survival in patients with reduced left ventricular ejection fractions and congestive heart failure. *N. Engl. J. Med.* **325**, 293–302. <https://doi.org/10.1056/NEJM199108013250501> (1991).
- Packer, M. *et al.* Effect of carvedilol on the morbidity of patients with severe chronic heart failure: results of the carvedilol prospective randomized cumulative survival (COPERNICUS) study. *Circulation* **106**, 2194–2199. <https://doi.org/10.1161/01.cir.0000035653.72855.bf> (2002).
- Towbin, J. A. *et al.* Incidence, causes, and outcomes of dilated cardiomyopathy in children. *JAMA* **296**, 1867–1876. <https://doi.org/10.1001/jama.296.15.1867> (2006).
- Kantor, P. F., Abraham, J. R., Dipchand, A. I., Benson, L. N. & Redington, A. N. The impact of changing medical therapy on transplantation-free survival in pediatric dilated cardiomyopathy. *J. Am. Coll. Cardiol.* **55**, 1377–1384. <https://doi.org/10.1016/j.jacc.2009.11.059> (2010).
- Boisson, B. *et al.* Immunodeficiency, autoinflammation and amylopectinosis in humans with inherited HOIL-1 and LUBAC deficiency. *Nat. Immunol.* **13**, 1178–1186. <https://doi.org/10.1038/ni.2457> (2012).
- Nilsson, J. *et al.* Polyglucosan body myopathy caused by defective ubiquitin ligase RBCK1. *Ann. Neurol.* **74**, 914–919. <https://doi.org/10.1002/ana.23963> (2013).
- Krenn, M. *et al.* Mutations outside the N-terminal part of RBCK1 may cause polyglucosan body myopathy with immunological dysfunction: expanding the genotype-phenotype spectrum. *J. Neurol.* **265**, 394–401. <https://doi.org/10.1007/s00415-017-8710-x> (2018).
- Kirisako, T. *et al.* A ubiquitin ligase complex assembles linear polyubiquitin chains. *EMBO J.* **25**, 4877–4887. <https://doi.org/10.1038/sj.emboj.7601360> (2006).
- Iwai, K., Fujita, H. & Sasaki, Y. Linear ubiquitin chains: NF-κB signalling, cell death and beyond. *Nat. Rev. Mol. Cell. Biol.* **15**, 503–508. <https://doi.org/10.1038/nrm3836> (2014).
- Sasaki, K. & Iwai, K. Roles of linear ubiquitylation, a crucial regulator of NF-κB and cell death, in the immune system. *Immunol. Rev.* **266**, 175–189. <https://doi.org/10.1111/imr.12308> (2015).
- Fujita, H. *et al.* Cooperative domain formation by homologous motifs in HOIL-1L and SHARPIN plays a crucial role in LUBAC stabilization. *Cell Rep.* **23**, 1192–1204. <https://doi.org/10.1016/j.celrep.2018.03.112> (2018).
- Peltzer, N. *et al.* LUBAC is essential for embryogenesis by preventing cell death and enabling haematopoiesis. *Nature* **557**, 112–117. <https://doi.org/10.1038/s41586-018-0064-8> (2018).
- Fuseya, Y. *et al.* The HOIL-1L ligase modulates immune signalling and cell death via monoubiquitination of LUBAC. *Nat. Cell. Biol.* **22**, 663–673. <https://doi.org/10.1038/s41556-020-0517-9> (2020).
- Kodo, K. *et al.* iPSC-derived cardiomyocytes reveal abnormal TGF-β signalling in left ventricular non-compaction cardiomyopathy. *Nat. Cell. Biol.* **18**, 1031–1042. <https://doi.org/10.1038/ncb3411> (2016).
- Hinson, J. T. *et al.* HEART DISEASE. Titin mutations in iPSC cells define sarcomere insufficiency as a cause of dilated cardiomyopathy. *Science* **349**, 982–986. <https://doi.org/10.1126/science.aaa5458> (2015).
- Streckfuss-Bömeke, K. *et al.* Severe DCM phenotype of patient harboring RBM20 mutation S635A can be modeled by patient-specific induced pluripotent stem cell-derived cardiomyocytes. *J. Mol. Cell. Cardiol.* **113**, 9–21. <https://doi.org/10.1016/j.yjmcc.2017.09.008> (2017).
- Li, X. *et al.* Overexpression of SerpinE2/protease nexin-1 contribute to pathological cardiac fibrosis via increasing collagen deposition. *Sci. Rep.* **6**, 37635. <https://doi.org/10.1038/srep37635> (2016).
- Zhou, J. *et al.* Loss of adult cardiac myocyte GSK-3 leads to mitotic catastrophe resulting in fatal dilated cardiomyopathy. *Circ. Res.* **118**, 1208–1222. <https://doi.org/10.1161/CIRCRESAHA.116.308544> (2016).
- Hedberg-Oldfors, C. & Oldfors, A. Polyglucosan storage myopathies. *Mol. Aspects Med.* **46**, 85–100. <https://doi.org/10.1016/j.mam.2015.08.006> (2015).
- Schoser, B. *et al.* Unclassified polysaccharidosis of the heart and skeletal muscle in siblings. *Mol. Genet. Metab.* **95**, 52–58. <https://doi.org/10.1016/j.ymgme.2008.07.005> (2008).
- Guo, Y. & Pu, W. T. Cardiomyocyte maturation: New phase in development. *Circ. Res.* **126**, 1086–1106. <https://doi.org/10.1161/CIRCRESAHA.119.315862> (2020).

25. Leone, M., Magadum, A. & Engel, F. B. Cardiomyocyte proliferation in cardiac development and regeneration: A guide to methodologies and interpretations. *Am. J. Physiol. Heart Circ. Physiol.* **309**, H1237–1250. <https://doi.org/10.1152/ajpheart.00559.2015> (2015).
26. Derks, W. & Bergmann, O. Polyploidy in cardiomyocytes: Roadblock to heart regeneration?. *Circ. Res.* **126**, 552–565. <https://doi.org/10.1161/CIRCRESAHA.119.315408> (2020).
27. Stopp, S. *et al.* Deletion of Gas2l3 in mice leads to specific defects in cardiomyocyte cytokinesis during development. *Proc. Natl. Acad. Sci. USA* **114**, 8029–8034. <https://doi.org/10.1073/pnas.1703406114> (2017).
28. Wu, M. *et al.* LUBAC controls chromosome alignment by targeting CENP-E to attached kinetochores. *Nat. Commun.* **10**, 273. <https://doi.org/10.1038/s41467-018-08043-7> (2019).
29. Craske, B. & Welburn, J. P. I. Leaving no-one behind: How CENP-E facilitates chromosome alignment. *Essays Biochem.* **64**, 313–324. <https://doi.org/10.1042/EBC20190073> (2020).
30. Nakagawa, M. *et al.* A novel efficient feeder-free culture system for the derivation of human induced pluripotent stem cells. *Sci. Rep.* **4**, 3594. <https://doi.org/10.1038/srep03594> (2014).
31. Tsurumi, F. *et al.* The intracellular Ca²⁺ concentration is elevated in cardiomyocytes differentiated from hiPSCs derived from a Duchenne muscular dystrophy patient. *PLoS One* **14**, e0213768. <https://doi.org/10.1371/journal.pone.0213768> (2019).
32. Yoshinaga, D. *et al.* Phenotype-based high-throughput classification of long QT syndrome subtypes using human induced pluripotent stem cells. *Stem Cell Rep.* **13**, 394–404. <https://doi.org/10.1016/j.stemcr.2019.06.007> (2019).
33. Lian, X. *et al.* Directed cardiomyocyte differentiation from human pluripotent stem cells by modulating Wnt/ β -catenin signaling under fully defined conditions. *Nat. Protoc.* **8**, 162–175. <https://doi.org/10.1038/nprot.2012.150> (2013).
34. Tohyama, S. *et al.* Distinct metabolic flow enables large-scale purification of mouse and human pluripotent stem cell-derived cardiomyocytes. *Cell Stem Cell* **12**, 127–137. <https://doi.org/10.1016/j.stem.2012.09.013> (2013).
35. Hoshi, T. *et al.* Mesdc2 plays a key role in cell-surface expression of Lrp4 and postsynaptic specialization in myotubes. *FEBS Lett.* **587**, 3749–3754. <https://doi.org/10.1016/j.febslet.2013.10.001> (2013).
36. Shahini, A. *et al.* NANOG restores the impaired myogenic differentiation potential of skeletal myoblasts after multiple population doublings. *Stem Cell Res.* **26**, 55–66. <https://doi.org/10.1016/j.scr.2017.11.018> (2018).
37. Lou, W. *et al.* Loss of tafazzin results in decreased myoblast differentiation in C2C12 cells: A myoblast model of Barth syndrome and cardiolipin deficiency. *Biochim. Biophys. Acta Mol. Cell Biol. Lipids* **857–865**, 2018. <https://doi.org/10.1016/j.bbalip.2018.04.015> (1863).
38. Reimand, J. *et al.* Pathway enrichment analysis and visualization of omics data using g:Profiler, GSEA, cytoscape and Enrichment-Map. *Nat. Protoc.* **14**, 482–517. <https://doi.org/10.1038/s41596-018-0103-9> (2019).

Acknowledgements

We are grateful to Dr. Yuji Yamanashi for providing C2C12 cells, Kumi Kodama for assisting with preparation and performance of the experiments, and Dr. Tomohiro Morio for recruiting a patient. Preparation of paraffin-embedded sections and H&E staining were supported by the Anatomic Pathology Center of the Graduate School of Medicine of Kyoto University.

Author contributions

K.A., S.B., M.K.S., K.I., and J.T. designed the experiments and the overall study. K.A. and S.B. wrote the manuscript. K.A., H.F., and Y.F. generated Hoil-11-KO C2C12 cells. K.A., D.Y., K.M., T.T., and T.H. performed the experiments. K.A. and H.K. performed the bioinformatics analysis. All authors discussed the results, and helped to prepare and edit the article.

Funding

This work was supported by the Fujiwara Memorial Foundation (to KA (2020)), the Takeda Science Foundation (to TT (2017)), Grants-in-Aid for Scientific Research (to SB (20K08421) and SB (23K07529)), the Core Center for Regenerative Medicine and Cell and Gene Therapy (JP23bm1323001) from the Japan Agency for Medical Research and Development (AMED) (to M.K.S), and a grant from the iPS Cell Research Fund (to M.K.S).

Competing interests

The authors declare no competing interests.

Additional information

Supplementary Information The online version contains supplementary material available at <https://doi.org/10.1038/s41598-024-57504-1>.

Correspondence and requests for materials should be addressed to S.B.

Reprints and permissions information is available at www.nature.com/reprints.

Publisher's note Springer Nature remains neutral with regard to jurisdictional claims in published maps and institutional affiliations.



Open Access This article is licensed under a Creative Commons Attribution 4.0 International License, which permits use, sharing, adaptation, distribution and reproduction in any medium or format, as long as you give appropriate credit to the original author(s) and the source, provide a link to the Creative Commons licence, and indicate if changes were made. The images or other third party material in this article are included in the article's Creative Commons licence, unless indicated otherwise in a credit line to the material. If material is not included in the article's Creative Commons licence and your intended use is not permitted by statutory regulation or exceeds the permitted use, you will need to obtain permission directly from the copyright holder. To view a copy of this licence, visit <http://creativecommons.org/licenses/by/4.0/>.

© The Author(s) 2024, corrected publication 2024